This is an Author's Accepted Manuscript of an article published in
International Journal of Remote Sensing,
Vol. 35, No. 10, pages 3459-3481. 2014.

Available online at:
http://dx.doi.org/10.1080/01431161.2014.904971

International Journal of Remote Sensing
Vol. 00, No. 00, 00 Month 201X, 1–26

ORIGINAL ARTICLE

Intercomparison of wave data obtained from single high-frequency radar, in-situ observation and model prediction

Yukiharu Hisaki[a]*

[a] *Department of Physics and Earth Sciences, University of the Ryukyus. 1 Aza-Senbaru, Nishihara-cho, Okinawa, Japan*

(*submitted November 2012*)

Wave data near the coast estimated from high-frequency (HF) radar are intercompared with in-situ and model-predicted wave data. The comparisons are useful since the in-situ wave data are limited to the main wave parameters and the observation is limited to a single point. The agreement between in-situ and model-predicted wave heights is reasonable, considering the accuracy of the model input wind. The agreement between radar-estimated and model-predicted wave energy in the intermediate frequency band, which is the most energetic frequency band, is better than that in the low or high frequency bands. On the other hand, the agreement between the radar-estimated and model-predicted wave direction is the best in the high frequency band, which is the band closest to the Bragg frequency. The spatial distribution of the radar-estimated wave heights during the observation period is similar to that of the model-predicted wave height in the limited area.

Keywords: Wave height; HF radar; Doppler spectrum; Numerical modeling; Wave spectrum

1. Introduction

The high-frequency (HF) ocean radar system is a promising tool for observing coastal surface currents and waves. There are many applied studies on coastal processes using HF radar-derived surface currents (e.g., Matthews et al. (1993); Son et. al. (2007); Hisaki and Imadu (2009); Muscarella et. al. (2011)). On the other hand, studies on coastal processes using HF radar-derived surface wave data are scarce, because it is difficult to estimate surface wave fields from HF radar.

However, it is possible to estimate ocean wave spectra near the coast using HF radar, which radiates the high-frequency radio waves to the sea surface and receives the backscattered signals. Doppler spectra are obtained from the backscattered signals, and ocean wave spectra are estimated on the basis of the integral equation, which relates the ocean wave spectrum to the Doppler spectrum (e.g., Lipa and Barrick (1986); Wyatt (1990); Hisaki (1996); Hashimoto et al. (2003)). Although ocean directional wave spectra are estimated using the dual HF radar systems, it is useful to estimate directional wave spectra by using single HF radar systems, because it is possible that one of the HF radar systems will be inoperable or that

*Corresponding author. Email: hisaki@sci.u-ryukyu.ac.jp

Doppler spectra from one of the HF radar systems will be affected by a large amount of noise.

In previous studies, only wave heights and periods were estimated by semi-empirical methods using a single HF radar system (e.g., Haus et al. (2010); Wyatt (2002)). On the other hand, there are methods which can be used to estimate a wave directional spectrum by using a single radar system (e.g., de Valk C et. al. (1999); Hisaki (2006)). These methods use the energy balance equation under the assumption of stationarity, along with the integral equation of the Doppler spectrum. Hisaki (2005, 2009) compared radar-estimated wave data observed by the Port and Airport Research Institute (PARI) in Japan. However, their comparison was limited to wave heights (Hisaki (2006); Hisaki (2009)). The observed wave data accessible to the public were limited to key wave parameters such as wave height and direction. A comparison of radar-estimated wave data not only with in-situ observed wave data but also with model-predicted wave data would be useful to evaluate the accuracy of radar-estimated wave data. Although there have been intercomparisons of HF radar-estimated wave parameters for the dual radar system (Wyatt et al. (2003); Wyatt et al. (2011)), there have been no intercomparison studies that included model-predicted wave parameters for the single radar system.

The objective of this study was to investigate the accuracy of radar-estimated wave data by intercomparing in-situ observed wave data and model-predicted wave data. Section 2 describes the wave measurement by HF radar. The wave model is also described in Section 2. Section 3 presents the results of the intercomparison. The results are discussed in Section 4. The conclusions are summarized in Section 5.

2. Method

2.1 *Observation and analysis of HF radar Doppler spectra*

The observation of Doppler spectra by HF radar was conducted in 2000 and 2001 for about 1 month. Figure 1 shows the observation area. The observation area was the East China Sea near the island of Okinawa in Japan The observation periods were from October 21 to December 7, 2000 and from May 26 to July 2 in 2001. The location of the HF radar was (26.38° N, 127.73° E) in 2000 and (26.42° N, 127.72° E) in 2001. The observation is described in Hisaki (2009). The radar frequency was 24.515 MHz, and the Bragg frequency was $f_B = 0.505$ Hz. The temporal resolution of the radar system was two hours. Beam directions was from 199° to 281.5° from true north (T) in 2000 and from 197.5° to 280° T in 2001.

The Doppler spectra were significantly contaminated by external noise, and the signal to noise ratios (SNRs) of the Doppler spectra were very low. The second-order scattering peak levels in the best Doppler spectra were several decibels (dB) above the noise level. The SNRs in most of the Doppler spectra were lower than those of the best Doppler spectra (Hisaki (2009)). The 3 (range) $\times$ 3 (beam) = 9 Doppler spectra were averaged in space, and the Doppler spectra were estimated on the 16 radial grid points in Figure 1a and b (Hisaki (2009)). The ocean wave spectral resolutions were 1.15 for frequencies (ratio of adjacent frequencies) and 20° for directions.

The equations to estimate wave spectra are equations of first- and second-order radar cross sections, energy balance equations and the regularization constraints. The unknowns to be estimated are spectral values and sea surface wind vectors (speeds and directions). The wind vectors are included in the energy balance equations and the regularization constraints. The number of equations are larger than

those of unknowns to be estimated. The unknowns are estimated by seeking the minimum of the objective function which is defined as the sum of weighted squares of the equations. This minimization problem is solved iteratively. The details of the method for estimating wave spectra are described in Hisaki (2006). The method for the quality control of spectra is also described in Hisaki (2009). The water depth is not considered in this method. Some of the low SNR Doppler spectra were not used to estimate wave spectra. The number of time series was 93 in 2000 and 190 in 2001.

2.2 *In-situ observation*

Wave heights and periods were observed by an Ultrasonic Wave gauge (USW) at 2-hour intervals. Wave directions were observed by a Current Meter Type Wave Direction Gauge (CWD) at 2-hour intervals. The surface elevations and orbital motions are observed for 20 minutes at 0.5-second intervals. Significant wave heights and periods are estimated by the zero-up-crossing method. Mean wave directions are estimated from values of covariances of orbital motions (Kawai et al. (2010)). The location of the USW was (26.26° N, 127.65° E) and the water depth was 53 m. The location of the CWD was (26.26° N, 127.66° E), and the water depth was 38 m. The number of time series during the HF radar observation period was 565 in 2000 and 451 in 2001.

The position of the wind station was (26.21° N, 127.69° E) on Okinawa island, and the elevation of the station from the sea surface was 28 m. The elevation of the anemometer from the ground was 48 m. The time, speed and directional resolution of the observed winds were 10 minutes, 1 m/s and 22.5°, respectively. The winds were averaged for 1 hour.

2.3 *Wave model*

The wave spectra were predicted by solving the energy balance equation as

$$\frac{\partial F}{\partial t} + \nabla \cdot (\mathbf{C}_g F) = S \tag{1}$$

where $F = F(f, \theta, \mathbf{x}, t)$ is the wave spectrum at the position $\mathbf{x}$, t is the time, f is the wave frequency, θ is the wave direction with respect to the eastward direction (counterclockwise is positive), ∇ is the horizontal gradient, $\mathbf{C}_g$ is the group velocity vector, and S is the source function as

$$S = S_{in} + S_{ds} + S_{nl} + S_{bt} \tag{2}$$

Equation (2) represents source terms for spectral wave energy due to the influence of wind (S_{in}), wave breaking (S_{ds}), nonlinear interactions (S_{nl}), and shallow-water processes (S_{bt}). The parameterization of the source function is the same as that of WAM (Wave Modeling) cycle-3 (WAMDI Group (1988)). However, the source function for wind input S_{in} was calculated for both Snyder's parameterization (Snyder et. al. 1981) and Jannsen's parameterization (Janssen 1991). The water depth is considered in the wave model.

The wave spectra were calculated by the nested grid: The coarse grid area was from 125.55° E to 128° E and from 23.95° N to 28.9° N with the spatial resolution of 0.05° (Figure 1c). The fine grid area was from 127.15° E to 127.9° and 26.1°N

from 26.6° N with the spatial resolution of 0.01° (Figure 1a and b). The time step was 240 s for the coarse grid, and 30 s for the fine grid. The wave frequency resolution (ratio of adjacent frequencies) was 1.1, and the resolution of the wave direction was 15°, both of which were finer than those of the HF radar-estimated wave spectra.

Objective analyzed surface winds from the Japan Meteorological Agency (JMA) data were used to predict wave spectra. The spatial and temporal resolutions for wind data from 2000 were 20 km and 12 hours, respectively, and these data are termed regional analysis (RANAL) data. The spatial and temporal resolutions for wind data from 2001 were 10 km and 6 hours, respectively, and these data are termed meso-scale analysis (MANAL) data. The objectively analysed data is described in Section 2.4. The wind data were linearly interpolated with respect to position and time.

The significant wave heights H, mean periods T_m, mean directions θ_m, frequency spectra $P(f)$ were calculated from model-predicted and radar-estimated wave spectra as

$$H = 4E^{1/2} \tag{3}$$

$$E = \int_0^{f_{max}} \int_{-\pi}^{\pi} F(f,\theta) d\theta df = \int_0^{f_{max}} P(f) df \tag{4}$$

$$T_m = E^{-1} \int_0^{f_{max}} f^{-1} P(f) df \tag{5}$$

$$\theta_m = \mathrm{atan}(Q_s Q_c^{-1}) \tag{6}$$

$$Q_c = \int_0^{f_{max}} \int_{-\pi}^{\pi} \cos\theta F(f,\theta) d\theta df \tag{7}$$

$$Q_s = \int_0^{f_{max}} \int_{-\pi}^{\pi} \sin\theta F(f,\theta) d\theta df. \tag{8}$$

The upper limits of integrations f_{max} in Eqs. (4)–(8) are 0.81 Hz for radar-estimated wave parameters and 0.56 Hz for model-predicted wave parameters.

2.4 *Objectively analysed wind data*

Optimal interpolation (OI) was used to merge the meteorological data into objective analysis data for 1999 and 2001 (JMA (2001); Shimbori (2003)). The four-dimensional variational method was not adopted in 2001. The merged data were land-, ship-, and buoy-based observations, but the sea surface winds recorded by the scatterometer were not used in 2001.

An optimum analysis of a field of model variables at grid points is

$$\mathbf{x}_a = \mathbf{x}_b + \mathsf{K}(\mathbf{y}_o - \mathsf{H}(\mathbf{x}_b)), \tag{9}$$

where $\mathbf{x}_b$ is an estimate of the model state provided by a previous forecast. The vector $\mathbf{y}_o$ is a set of observations of the same parameter as $\mathbf{x}_a$ and $\mathbf{x}_b$. The matrix H denotes interpolation operator from the model discretization to the observation points. The gain matrix K is given by equation (A6) in Bouttier and Courtier (1999).

The MANAL and RANAL data were used as initial conditions of the weather

forecast by the RSM (Regional Spectral Model) and MSM (Meso-Scale Model) of JMA. The "pre-run" was employed in the MANAL, whereas the OI was conducted in the hourly update cycle for the last 3-hour period preceding the analysis time. The initial condition of the 3-hour pre-run process was created by the interpolation from the RSM forecast data. The reason for the use of the pre-run was that the time to collect data for the forecast by the MSM, which should be reported promptly, was shorter than that for the forecast by the RSM (Kimura et al. (2001)). The RANAL data were derived by running the RSM and conducting the OI every 6 hours. The analyzed data were smoothed in the horizontal grid, because the observation points were unevenly distributed.

The smoothing of the MANAL and RANAL data was conducted until November 2003, but the effect of the smoothing on surface wind speeds was large around the coastline (Unpublished results, Numerical Prediction Division, Japan Meteorological Agency). The sea surface wind data by QuikSCAT had not been incorporated in 2001. The four-dimensional variational method was not adopted but the OI was adopted until May 2003 in RSM and February 2002 in MSM (Shimbori 2003).

3. Results

3.1 *Example of wave estimation*

Figure 2 shows an example of wave spectra at 14 JST, 5 June 2001 on the radial (HF radar-estimated spectra) and the regular (model-predicted spectra) grid points, which were the closest to the in-situ observation point. The distance of between the USW and the closest radar radial point is 0.7 km in 2000 and 1.1 km in 2001. The distance between the USW and the closest wave model grid point is 0.4 km.

Wave spectra estimated from the HF radar and predicted from Eq. (1) are shown in Figure 2. The wind inputs (S_{in}) are calculated from Snyder's parameterization (Snyder et. al. 1981) in Figure 2c and d. The parameterization of Janssen (1991) was also used to predict wave spectra. However, there were almost no differences in the predicted wave spectra between them. Therefore, only the cases of Snyder's parameterization are indicated in this paper.

Figure 2a shows an HF radar-estimated wave frequency spectrum $P(f)$, and Figure 2b shows an HF radar-estimated normalized directional distribution (%), which was estimated by dividing the wave spectrum $F(f,\theta)$ by the frequency spectrum $P(f)$, i.e., $F(f,\theta)/P(f)$. Figure 2c and d show a predicted wave frequency spectrum $P(f)$ and a normalized directional distribution $F(f,\theta)/P(f)$. The radar-estimated and model-predicted wave heights at the time were 0.86 m and 0.92 m, respectively, while the in-situ observed wave height was 0.47 m. Both the model-predicted and radar-estimated wave directions were northeastward. This is a typical example showing agreement between model-predicted and radar-estimated wave height, but there are differences in directional spectra.

The peak wave frequencies are different in Figure 2a and c. There is a local peak at (0.11 Hz, 0°) in Figure 2d. The value of $P(f)$ is less than 0.05 m^2s (Figure 2c), and the local peak level is small. If there is a swell as Figure 2d, the second-order Doppler peaks by the swell are between first-order peaks and the second-order peaks by the dominant wave in the Doppler spectrum. The second-order Doppler peak by the swell is much smaller than the first- and the second-order peaks, so it is difficult to retrieve the swell peak of the wave directional spectrum.

We can see the bimodality in Figure 2d. The local maxima of $F(f,\theta)$ for $f =$ 0.11 Hz can be seen at $\theta = 0°$ and at $\theta = 30°$. The direction resolution of the radar-

estimated wave spectrum is 20°, and it is too low to retrive the bimodal directional distribution as Figure 2d. The regularization constraint in the $f-\theta$ plain is used for wave estimation, and it is difficult to retrive the bimodal directional distribution as Figure 2d.

The wind direction changed from northwestward to northeastward during the period. The northwestward wind direction is the fetch-limited condition and northeastward wind direction is the fetch-unlimited condition in the in-situ observation point. The development of the wave spectrum is sensitive to the wind direction during the period. A possible explanation of the difference of peak wave frequencies is the difference of the model input wind direction and the true wind direction.

3.2 *Comparison of wave parameters*

Figure 3 depicts the time series of model-predicted wave heights (H_m), radar-estimated wave heights (H_r) and in-situ observed wave heights (H_o). The model-predicted wave heights were overestimated on October 27 and November 2, 2000. The model-predicted wave heights were also overestimated on May 31, and June 14, 2001. On the other hand, they were underestimated on November 18, 21 and 29, 2000. The model-predicted wave heights were often underestimated in 2000, and overestimated in 2001. A possible reason for this is discussed in section 4.1. The radar-estimated wave heights were also underestimated in 2000, and overestimated in 2001, which is discussed in section 4.2.

The radar-estimated wave heights were scattered temporally. Figure 4 shows a series of scatter diagrams plotting in situ, model-predicted and radar-estimated wave heights for both years, and Tables 1 and 2 summarize the comparison of wave parameters. The correlation coefficients (r) and rms differences between the model-predicted and in-situ observed wave parameters were estimated at the time when the waves were estimated from the radar. These values for the total HF radar observation period were also estimated.

Agreement between the radar-estimated and in-situ observed wave heights was the best among the pairs, while that between the radar-estimated and model-predicted wave heights was the worst. Both the radar and model tended to underestimate the wave heights for $H_o > 1$ m, while the tendency was more clear for the radar estimation.

Figure 5 shows the time series of model wind directions, radar-estimated wind directions and in-situ observed wind directions. Figure 6 shows the scatter diagram for these three time series. The model wind data were the objectively analysed surface winds from the JMA used to drive the wave prediction model. This is explained in Section 2.3. The wind data were linearly interpolated with respect to time when radar measurements were acquired. The location of radar-estimated wind directions was the radial grid point that was closest to the USW. The location of the model wind directions was the regular point that was the closest to the wind station. Values of directions in Figure 5 are added or subtracted by 360° for Figure 6, because the maximum difference of directions is 180°. The spatial variability of model wind directions was small. The rms difference between the observed wind direction and model (objectively analyzed) wind direction was 27.8°, which was associated with temporal variations of the observed winds.

The wind speeds were also estimated from the radar. However, there were no correlations between the radar-estimated wind speeds and in-situ observed wind speeds.

The mean wave directions are compared. Figure 7 shows the relationship be-

tween the threshold of in-situ observed wave heights (H_t) and rms differences of mean wave directions. For a given value of H_t, the rms difference of mean wave directions was obtained only in the case when the in-situ observed wave heights H_o were greater than H_t. For example, when $H_o \geq 0.6$ m, the rms differences between radar-estimated and in-situ observed mean wave directions, between radar-estimated and model-predicted mean wave directions, and between in-situ observed and model-predicted mean wave directions in 2001 (Figure 7b) are 58.3°, 65.8° and 45.7°, respectively. For the small wave heights, the accuracy of the wave direction estimated from the CWD was poor. The differences became smaller as the threshold became larger, which shows that the wave direction from the CWD was not accurate in the case of small wave height.

The comparisons of the wave periods are also summarized in Table 1 and 2. The wave period data supplied from the PARI is the significant wave period. The model-estimated and radar-estimated wave periods were spectral mean periods. Their correlations were smaller than those for the wave heights.

3.3 *Comparisons of wave spectra and spatial distribution.*

In order to compare wave spectral values, the wave energy was divided into three parts–low-, intermediate- and high- frequency wave heights, which were defined as

$$H(f_1, f_2) = 4\Big(\int_{f_1}^{f_2} P(f)df\Big)^{1/2}. \tag{10}$$

The low-, intermediate- and high-frequency ranges were $(f_1, f_2) = (0, 0.14)$, $(0.14, 0.3)$, and $(0.3, 0.5)$ Hz, respectively. Wave directions were also defined for the three wave frequency bands as

$$\theta_m(f_1, f_2) = \mathrm{atan}(Q_s(f_1, f_2)Q_c^{-1}(f_1, f_2)), \tag{11}$$

$$Q_c(f_1, f_2) = \int_{f_1}^{f_2}\int_{-\pi}^{\pi} \cos\theta F(f, \theta)d\theta df, \tag{12}$$

$$Q_s(f_1, f_2) = \int_{f_1}^{f_2}\int_{-\pi}^{\pi} \sin\theta F(f, \theta)d\theta df. \tag{13}$$

The upper frequency of the high-frequency band is 0.5 Hz, which is close to the Bragg frequency. The nonlinear inversion estimates spectral values at higher frequencies, while a linear inversion does not. The frequency ranges of the bands are determined so that most of the peak frequencies are in the intermediate frequency band. In addition, the frequency ranges of the bands are determined so that the bandwidths are not dissimilar. The ratios of model-predicted peak wave frequencies are in the low-, intermediate- and high- frequency bands are 33.2 %, 64.0 %, and 2.8 %, respectively. These boundaries of the frequency bands are appropriate.

Figure 8 shows examples of the comparison, and Table 3 and 4 are summaries of the comparison. The agreement of $H(f_1, f_2)$ was optimum for the intermediate frequency band, while the spectral mean wave direction was optimum for the high-frequency band. The correlation of wave height with $H(f_1, f_2)$ was the highest for the intermediate frequency in total, which is discussed in Section 4.3.

On the other hand, the wave direction for the high frequency range was the closest to the wind direction. The difference between the predicted and radar-estimated wave direction was lowest for the high frequency case, which is discussed

in Section 4.3.

Figure 9 shows the predicted mean wave height and radar-estimated mean wave height during the 2000 and 2001 experiments. The averaged periods of predicted mean wave heights were the same as those for the radar-estimated mean wave heights. The spatial variability of the radar-estimated wave heights was larger than that of the predicted wave heights. However, the features of spatial distribution patterns were similar: The local maxima of wave height can be seen near the radar position, and wave heights decreased with increasing distance offshore within the small area of 127.6° E–127.7° E and 26.3° N –26.4° N in 2000 (Figure 9a). The decrease in radar-estimated wave heights was more significant than that of the predicted wave heights. The local wave height maxima can also be seen near the radar position in both radar-estimated and model-predicted wave heights from the 2001 data. The wave height also decreases with increasing distance offshore within the limited area in that case.

4. Discussion

4.1 *Comparison of model and in-situ wave parameters*

We compared in-situ, model-predicted and HF radar-estimated wave data. Since the in-situ observed data were limited to single point observations, model-predicted data were used for the comparison. The Doppler spectra were significantly contaminated by noise: The SNR was at most several dB. The correlation between the model-predicted wave height and the in-situ observed wave height data was 0.67 for the total HF radar observation period, which is not high. The accuracy of the predicted wave height was dependent on wind accuracy. The correlation between model input wind speeds and in-situ observed wind speeds was 0.77. If the wave height is proportional to the square of wind speed, the correlation of 0.67 is reasonable. The correlation between the squares of model input wind speeds and model predicted wave heights at the wave observation point was 0.90, which shows that the wave height was almost proportional to the square of the wind speed. The observed wind data were not identical to the objective analysis surface wind data (Eq. (9)).

The model-input surface wind is less accurate, which is explained in Section 2.4. The difference between in-situ observed waves and model predicted waves originates from wind speed inaccuracies

Model-input wind direction errors are also sources of inaccurate predictions of wave heights, especially under fetch-limited conditions. For example, the predicted wave heights were overestimated on 14 June, 2001. The wind directions varied from 0° to 90° with respect to the eastward direction (counterclockwise is positive: for example, the direction of a northeastward wind is 45°.) on 14 June, 2001 (Figure 5). The black circles (model input wind directions) were below the solid line (observed wind directions) on 14 June, 2001 in Figure 5b. The observed wind directions were counterclockwise directions with respect to the model input wind directions on that day. This shows that the fetches for the observed wind directions were shorter than those for the model input wind directions (Figure 1). Therefore, the predicted wave heights were overestimated on 14 June, 2001.

On the other hand, the predicted wave heights were underestimated on 21 November, 2000. A storm associated with an atmospheric front was present in the East China Sea on 20 November, 2000. The maximum sea surface wind speed exceeded 25 m/s at (29° N, 125.5° E). The storm area is outside the computation area in

Figure 1c. The swell associated with the storm was not reproduced, and the predicted wave heights were underestimated. If the swell source is not included in the computation area, the predicted wave heights may be underestimated.

The effect of the swell on wave prediction is investigated. Wave periods in swell-dominated conditions are longer than those in wind-wave conditions. A linear regression line between common logarithms of observed wave heights ($\log_{10}(H_o)$) and that of observed mean wave periods ($\log_{10}(T_{ms})$) is estimated as

$$\log_{10}(T_{ms}) = \alpha \log_{10}(H_o) + \beta \tag{14}$$

from in-situ observed wave data, for which the values

$$q_s = \log_{10}(T_{ms}) - \alpha \log_{10}(H_o) - \beta \tag{15}$$

are defined. The value of q_s is larger as swell dominates. Figure 10 shows the relationship between the value of underestimation of model-predicted wave heights and numbers of data for $q_s > 0$ and $q_s < 0$. We counted the time series data for $q_s > 0$ (which is defined as Q_p) and $q_s < 0$ (which is defined as Q_n) satisfying

$$H_o - H_m > h_t, \tag{16}$$

where h_t is a parameter of a wave height difference. We plotted $Q_p = Q_p(h_t)$ and $Q_n = Q_n(h_t)$ as a function of h_t in Figure 10.

For example, the values Q_p and Q_n for $h_t = 0.5$ m are $Q_p = 65$ and $Q_n = 36$, respectively. The total number of time series data is 1065, and the number of time series data that satisfies $H_o - H_m \leq 0.5$ m is 964.

The value of Q_n is larger than Q_p for $h_t < 0.25$ m. Wave heights are frequently underpredicted or accurately predicted in the case of wind wave conditions. The value of Q_p is larger than Q_n for higher h_t. This shows that the swell-dominated condition is more frequent than the wind-wave condition in the cases where a wave height is under-predicted.

The difference between model-predicted and in-situ observed mean wave directions in 2000 are also larger than those in 2001 even for larger wave heights (Figure 7). This is also related to the prediction of the swell.

Figure 11 shows the relationship between the threshold of in-situ observed wave heights (H_t) and rms differences between model-predicted and in-situ observed mean wave directions for $q_s > 0$ (Eq. (15)) and $q_s < 0$ in 2000 and 2001. The rms differences for $q_s > 0$ are large even for larger H_t in 2000, which shows that swell directions in 2000 could not often be predicted.

4.2 *Comparison of wave parameters for other pairs*

The correlation between the radar-estimated wave height and the in-situ observed wave height data was 0.73. This value is not as high as the dual radar case (Wyatt et al. (2003); Wyatt et al. (2011)), but is comparable to other studies of the single radar case (Wyatt (2002); Haus et al. (2010)), in which correlations are from 0.7 to 0.8. The empirical correction factor for wave height was not used in the present method.

If the noise is not completely excluded, the wave height is overestimated. A possible explanation of the underestimation of wave height in 2000 is as follows: the Doppler frequencies of the second-order Doppler peaks associated with a swell

are close to the first-order peak Doppler frequencies. The first-order scattering of the Doppler spectrum is broadened by the current shear in the radar cell, and the separation of the second-order Doppler peaks from the first-order scattering fails: the second-order signal from the swell is included in the first-order part of the spectrum. In this case, the wave height is underestimated from the HF radar.

The difference between radar-estimated and in-situ observed mean wave directions in 2000 are also larger than those in 2001 even for larger wave heights (Figure 7). This is also related with the separation of the second-order Doppler peaks from the first-order scattering.

The difference between model-predicted and radar-estimated mean wave directions is the largest even for larger wave heights in 2000 (Figure 7). Swell directions in 2000 could not often be predicted as explained in Section 4.1. Swell signals in the second-order Doppler spectra are often included in the first order part of the Doppler spectra for 2000, the large difference being due to both of them.

4.3 *Comparisons of wave spectra*

The agreement of wave energy in the intermediate wave frequency band, which is the most energetic frequency band, was the best. The reason is that the second-order Doppler peaks by the dominant wave are the most robust to noise in the second-order Doppler spectrum. On the other hand, the agreement of the wave direction in the high frequency band was the best, because the high frequency wave direction was related to the wind direction. The response of wave direction in the high-frequency band to change in wind direction was quicker than that in the lower frequency band (e.g., Hasselmann et al. (1980)). The regularization constraints in the $f-\theta$ (wave frequency-wave direction) plane are used in the inversion method (Hisaki 2006). The spectral values of the neighbouring grid points in the $f-\theta$ plane are close to each other. The wave direction in the high frequency band is close to that of Bragg wavelength.

The upper frequency of the radar estimated wave spectrum is higher than the Bragg frequency (Sections 2.1 and 2.3). The wave direction of the Bragg wavelength is the most accurate, because the direction is estimated from first-order scattering, which is robust to noise. The wave direction at the higher frequency is close to the wave direction of the Bragg wavelength because of the rapid response to wind shift. The radar-estimated wave direction at the higher frequency is also close to the wave direction of the Bragg wavelength because of the regulatization constraints. Therefore, wave direction at the higher frequency band is the most accurate of the three bands. If the wave directional distribution is estimated only from second-order scattering, the result may not be true. However, the result is true for any HF radar wave estimation in the present method, because the first-order scattering is used for estimating the wave directional distribution.

4.4 *Comparisons of spatial distribution*

The spatial distribution patterns of radar-estimated mean wave heights were similar to those of model predicted mean wave heights in the limited area. The spatial patterns are similar to each other in the area from 127.6° E to 127.7° E and from 26.3° N to 26.4° N: The positions of the local maximum in the spatial distributions of the wave heights were close to each other. For example, the local maxima of wave heights can be seen at (26.35° N, 127.67°) in Figure 9a and b. The decrease in mean wave height, moving offshore from the local maxima, can be seen in both

radar-estimated and model-predicted wave heights within the limited area.

The similarity of the spatial distributions in the limited area is evaluated. The radar mean wave heights are interpolated in the $0.01^\circ \times 0.01^\circ$ regular grids, which are the same as the wave model grids. The spatial correlation coefficients between $\bar{H}_r(x, y)$ and $\bar{H}_m(x + d_x, y + d_y)$ in the range of $x_a \leq x \leq x_b$ and $y_a \leq y \leq y_b$ are calculated from the gridded mean wave heights, where $\bar{H}_r(x, y)$ is the mean radar wave height at the position (x, y), and $\bar{H}_m(x + d_x, y + d_y)$ is the the mean model wave height at the position $(x + d_x, y + d_y)$. The correlation coefficients r_c are calculated for various x_a, x_b, y_a, y_b, d_x and d_y. The number of grid points (N_c) for calculating the correlation is also estimated.

If we compare only for $\bar{H}_r(x, y)$ and $\bar{H}_m(x, y)$ in the area of $x_a \leq x \leq x_b$ and $y_a \leq y \leq y_b$, the correlation is sensitive to the positions of the local maxima of $\bar{H}_r(x, y)$ and $\bar{H}_m(x, y)$. Although the spatial patterns of $\bar{H}_r(x, y)$ and $\bar{H}_m(x, y)$ seem to be similar, the correlation may be small. Therefore, it is better to $\bar{H}_r(x, y)$ and $\bar{H}_m(x + d_x, y + d_y)$ for comparing the spatial patterns to judge as being similar with each other. The magnitude of (d_x, d_y) must be low.

The spatial correlation coefficients for the total HF radar observation area and $(d_x, d_y) = (0, 0)$ are $r_c = 0.38$ in 2000 and $r_c = 0.07$, respectively. The maximum r_c as a function of (d_x, d_y) for the total HF radar observation area is $r_c = 0.48$ at $(d_x, d_y) = (0.02^\circ, -0.03^\circ)$ in 2000, and $r_c = 0.49$ at $(d_x, d_y) = (0.03^\circ, -0.05^\circ)$ in 2001. The values of $(d_x, d_y) = (0.02^\circ, -0.03^\circ)$ and $(0.03^\circ, -0.05^\circ)$ correspond to the distance of 3.9 km and 6.3 km, respectively. This means that the similarity between Figure 9a and b is very close to that between Figure 9c and d.

The maximum r_c as a function of (x_a, x_b, y_a, y_b) and (d_x, d_y) for $N_c \geq 100$ is 0.77 at (x_a, x_b, y_a, y_b) = (127.57° E, 127.65° E, 26.25° N, 26.37° N) and (d_x, d_y) = $(0.03^\circ, 0^\circ)$ in 2000. The maximum r_c for $N_c \geq 100$ is 0.71 at (x_a, x_b, y_a, y_b) = (127.56° E, 127.67° E, 26.24° N, 26.39° N) and $(d_x, d_y) = (0.02^\circ, -0.03^\circ)$ in 2001.

The correlation between $\bar{H}_r(x, y)$ in the range of 127.57° E to 127.65° E and 26.25° N to 26.37° N (Figure 9b) and $\bar{H}_m(x, y)$ in the range of 127.6° E to 127.68° E and 26.25° N to 26.37° N (Figure 9a) is 0.77 in 2000.

The correlation between $\bar{H}_r(x, y)$ in the range of 127.56° E to 127.67° E and 26.24° N to 26.39° N (Figure 9d) and $\bar{H}_m(x, y)$ in the range of 127.58° E to 127.69° E and 26.21° N to 26.36° N (Figure 9d) is 0.71 in 2001. It is shown that the spatial pattern of radar-estimated mean wave heights is similar to that of model predicted mean wave heights in the limited area.

The water depth changes significantly in the local maxima area of predicted wave heights (Figure 1). A possible reason for the local maxima of wave heights is that the long waves were controlled by the bottom topography and the wave energy was concentrated in the local maxima region.

4.5 *Comparison of winds*

The rms difference between the observed wind direction and radar wind direction was 40.2°. This difference is larger than that reported by Hisaki (2002), which compared wave directions of Bragg wavelength to those of the land-based station. The temporal variability of model winds is less than that of in-situ winds. The temporal variability of radar winds is less than that of in-situ winds. The temporal variability of the differences between model and radar winds is less than that of the differences between in-situ and radar winds. Therefore, the rms difference between the model and radar wind directions was less than that between in-situ and radar wind directions.

The initial estimate for wind direction was estimated from the first-order scattering, and this was robust to the noise in the Doppler spectrum. The radar-estimated wind directions were close to the initial estimate. Although the accuracy of wind directions estimated from the single radar is not as high as that from the dual radar, the single radar system used to estimate wind directions is useful if we can use only the single radar system.

The difference between radar-estimated and in-situ wind direction in 2000 is less than that in 2001, while the difference of wave heights in 2000 is larger than that in 2001. Errors of wave heights are associated with noises in Doppler spectra, while the differences in wind direction are due to the spatial and temporal variability of wind direction. The separation of first-order scattering from second-order scattering is more critical to wave height estimation than to wind direction estimation, because second-order scattering is much smaller than first-order scattering.

The root-mean-squares of $\theta_{ws}(k+1)-\theta_{ws}(k)$, where θ_{ws} is in-situ observed wind directions and k is the time series number at 2-hour intervals, are 16.8° in 2000 and 25.9° in 2001, respectively.

The root-mean-squares of $\theta_{ws}(k)-\theta'_{ws}(k)$, where θ'_{ws} is wind directions at the station at (26.21°N, 127.36°E), which is on a small island west of the HF radar observation area, are also estimated. They are 11.4° in 2000 and 16.5° in 2001, respectively. The temporal variation in wind is related to its spatial variation, because these variations are due to atmospheric disturbances.

When wind direction shifts, the mean wave direction of Bragg wavelength is not shifted simultaneously, and wind direction is different from the mean wave direction of Bragg wavelength. This difference is considered in the present method: the initial estimate of the wind direction for the iteration of the minimization problem (Section 2.1) is the mean wave direction of the Bragg wavelength, which is estimated from the first-order scattering. The wind direction is corrected from the estimation by the iteration: however, the correction is small. We must improve the correction method for this difference.

Wind speeds could not be estimated accurately from the HF radar in the present study. Wind speed can be evaluated from a wind wave spectrum. which consists of a wind wave spectrum and swell components. If a wind wave spectrum could be isolated from a radar-estimated wave spectrum, it might be possible to estimate wind speed from the isolated wind wave spectrum and the fetch inferred from the wind direction estimated from the HF radar.

5. Conclusion

The main conclusions are summarized as follows:

(1) The single HF radar system can be used as a substitution for the dual radar system for estimating wave heights and wind directions but accuracy will be lower than with the dual HF radar system.
(2) The agreement between radar-estimated and model-predicted wave energy in the intermediate frequency band, which is the most energetic frequency band, is better than that in the low or high frequency bands. On the other hand, the agreement between radar-estimated and model-predicted wave direction is the best in the high frequency band, which is the band closest to the Bragg frequency.
(3) The spatial variability of the mean radar-estimated wave height is similar to that of model-predicted wave height in the limited area: local maxima of

mean wave heights in both distributions are found at positions close to each other.

(4) The errors of radar-estimated wave heights are associated with noise in Doppler spectra or broadening of first-order scattering, while those of radar-estimated wind directions are associated with the spatial and temporal variability of winds. The errors of the two parameters are not related. On the other hand, accurate model input wind directions are critical to predicting wave heights near small islands.

The dual radar system can improve the accuracy of wave estimation. However, if the SNR of the Doppler spectrum of one of the dual radars is low, wave height accuracy will be compromised. The method for selecting optimum wave data from the single and dual radar-derived wave data should be developed in the future.

Acknowledgments

This study was financially supported by a Grant-in-Aid for Scientific Research (C-2) from the Ministry of Education, Culture, Sports, Science, and Technology of Japan (20540429). The GFD DENNOU Library (available online at http://www.gfd-dennou.org/arch/dcl/) was used for drawing the figures. Comments from anonymous reviewers were helpful in improving the manuscript.

References

Bouttier, F. and P. Courtier, 1999 : Data assimilation concepts and methods, Meteorological Training Course Lecture Series, ECMWF, 59pp.

Kimura K, T. Tsuyuki, K. Koizumi, T. Matsumura, H. Goda, R. Taira, M. Kunitsugu, S. Yamada, M. Nishijima, 2001: On the seventh generation Numerical Analysis and Prediction System (NAPS). Weather Service Bulletin JMA, 68, 25-76 (in Japanese).

Hashimoto N., L. R. Wyatt, and S. Kojima, 2003: Verification of a Bayesian method for estimating directional spectra from HF radar surface backscatter. Coastal Engineering Journal, 45, 255-274.

Hasselmann, K., M. Dunckel, and J. A. Ewing, 1980: Directional wave spectra observed during JONSWAP 1973. Journal of Physical Oceanography, 10, 1264-1280.

Haus, B. K., L. K. Shay, P. A. Work, G. Voulgaris, R. J. Ramos and J. Martinez-Pedraja, 2010. Wind speed dependence of single-site wave-height retrievals from high-frequency radars. Journal of Atmospheric and Oceanic Technology, 27, 1381-1394.

Hisaki. Y., 1996. Nonlinear inversion of the integral equation to estimate ocean wave spectra from HF radar. Radio Science. 31, 25–39.

Hisaki, Y., 2002: Short-wave directional properties in the vicinity of atmospheric and oceanic fronts. Journal of Geophysical Research. **107,** 11, doi:10.1029/2001JC000912.

Hisaki, Y., 2005: Ocean wave directional spectra estimation from an HF ocean radar with a single antenna array: Observation. Journal of Geophysical Research. **110,** 10, doi: 10.1029/2005JC002881.

Hisaki, Y., 2006. Ocean wave directional spectra estimation from an HF ocean radar with a single antenna array: Methodology. Journal of Atmospheric and Oceanic Technology, 23, 268–286.

Hisaki Y., 2009. Quality control of surface wave data estimated from low signal-to-noise ratio HF radar Doppler spectra. Journal of Atmospheric and Oceanic Technology, 26,. 2444-2461.

Hisaki, Y., and C. Imadu 2009, The southward recirculation of the East China Sea Kuroshio west of the Okinawa Island, Journal of Geophysical Research, doi:10.1029/2008JC004943.

Kawai, H., Satoh M., and Kawaguchi K., 2010, Annual Report on Nationwide ocean wave information network for ports and harbours (NOWPHAS 2008). Technical Note of the Port and Airport Research Institute, No 1209, 93 pp (in Japanese).

Janssen P. A. E. M., 1991. Quasi-linear theory of wind wave generation applied to wave forecasting. Journal of Physical Oceanography, 21, 1631-1642.

Japan Meteorological Agency, 2001: Annual WWW Technical Progress Report on the Global Data Processing System 2001. GDPS Technical Progress Report Series No. 11, WMO/TD-No. 1115. available from `http://www.wmo.int/pages/prog/www/DPFS/ProgressReports/index-2001.html`

Lipa, B.J., and D. E. Barrick, 1986, Extraction of sea state from HF radar sea echo: Mathematical theory and modeling. Radio Science, 1, 81-100.

Matthews J. P., A. D. Fox and D. Prandle, 1993. Radar observation of an along-front jet and transverse flow convergence associated with a North Sea front. Continental Shelf Research. 109-130.

Muscarella P. A. , N. P. Barton, B. L. Lipphardt Jr., D. E. Veron, K. C. Wong, and A. D. Kirwan Jr. 2011: Surface currents and winds at the Delaware Bay mouth. Continental Shelf Research. 31, 1282-1293.

Shimbori, T., 2003: Operational implementation of the four-dimensional variational method into JMA regional analysis. Tenki, 50, 721 -727 (in Japanese).

Snyder, R. L., F. W. Dobson J. A. Elliott and R. B. Long, 1981: Array measurements of atmospheric pressure fluctuations above surface gravity waves. Journal of Fluid Mechanics. 102, 1-59.

Son, Y. T., S. H. Lee, C. S. Kim, J. C. Lee, G. H. Lee, 2007: Surface current variability in the Keum River Estuary (South Korea) during summer 2002 as observed by high-frequency radar and coastal monitoring buoy. Continental Shelf Research, 27, 43-63 .

de Valk C, Reniers A, Atanga J, Vizinho A., and Vogelzang J., 1999. Monitoring surface waves in coastal waters by integrating HF radar measurement and modelling. Coastal Engineering. 37, 431–453.

WAMDI Group, 1988. The WAM model. A third generation ocean wave prediction model. Journal of Physical Oceanography 18, 1775-1809.

Wyatt, L. R., 1990, A relaxation method for integral inversion applied to HF radar measurement of the ocean wave directional spectra. International Journal of Remote Sensing, 11, 1481-1494.

Wyatt L. R., 2002, An evaluation of wave parameters measured using a single HF radar system. Canadian Jornal of Remote Sensing. 28, 205–218.

Wyatt L. R., J.J. Green, K.-W. Gurgel, J. C. NietoBorge, K. Reichert, K. Hessner, H. Günther, W. Rosenthal, Ø. Saetra and M. Reistad, 2003. Validation and intercomparisons of wave measurements and models during the EuroROSE experiments, Coastal Engineering. 48, 1–28.

Wyatt L. R., J. J. Green, A. Middleditch, 2011. HF radar data quality requirements for wave measurement. Coastal Engineering. 58, 327–336.

Figures and captions

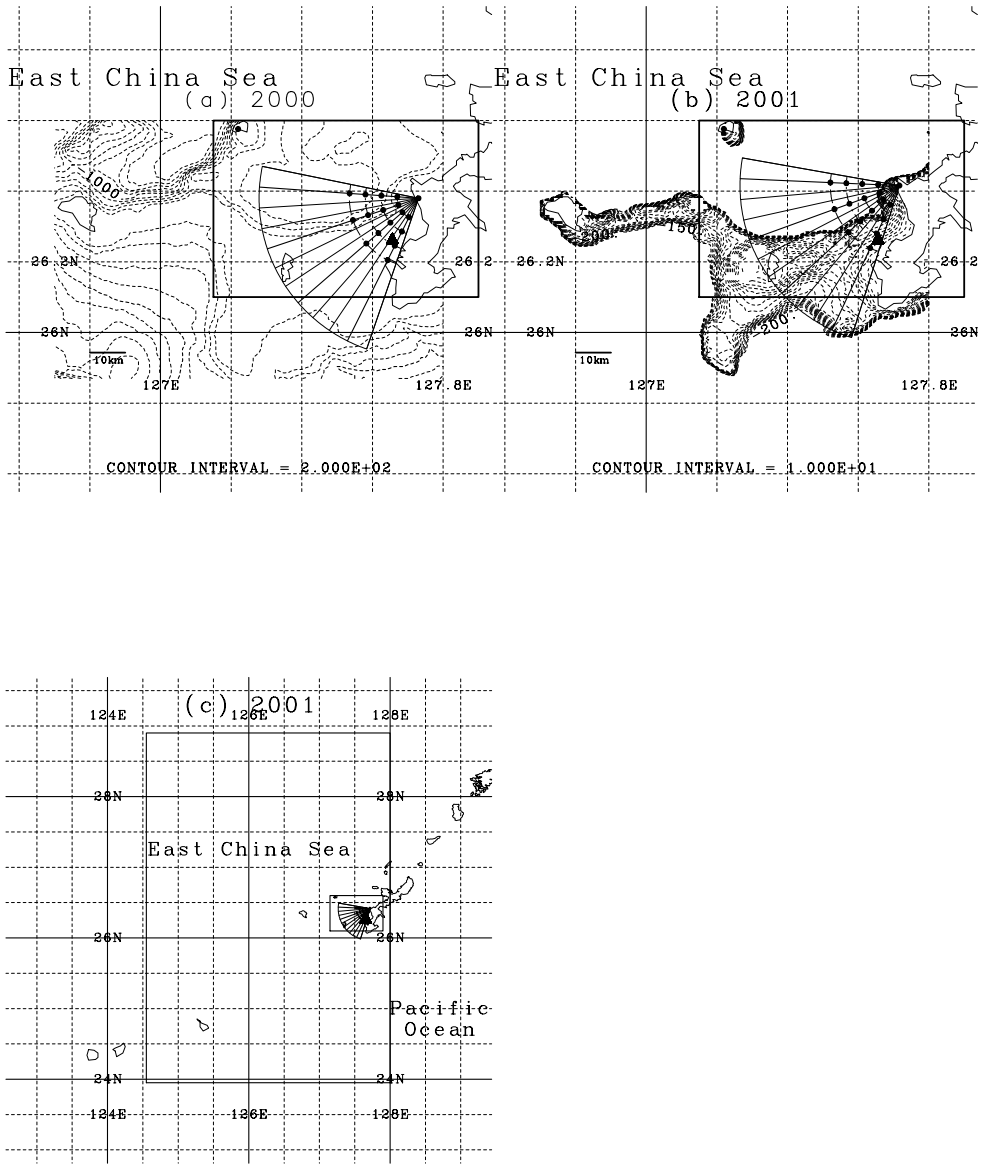

Figure 1. HF radar observation area in (a) 2000 and (b) 2001 and (c) the model computation area. The location of USW (26.26° N, 127.65° E) was ▲. The depth contours (dashed lines in (a) and (b)) are 200 m step in (a), and 10 m step in (b). The maximum depth contour in (b) is 200 m. The area from 125.55° E to 128° E and from 23.95° N to 28.9° N (rectangle) in (c) is the computation area of wave spectra at low spatial resolution (0.05°), and the area from 127.15° E to 127.9° and 26.1°N from 26.6° N (rectangle) in (a), (b) and (c) is the computation area of wave spectra at high spatial resolution (0.01°).

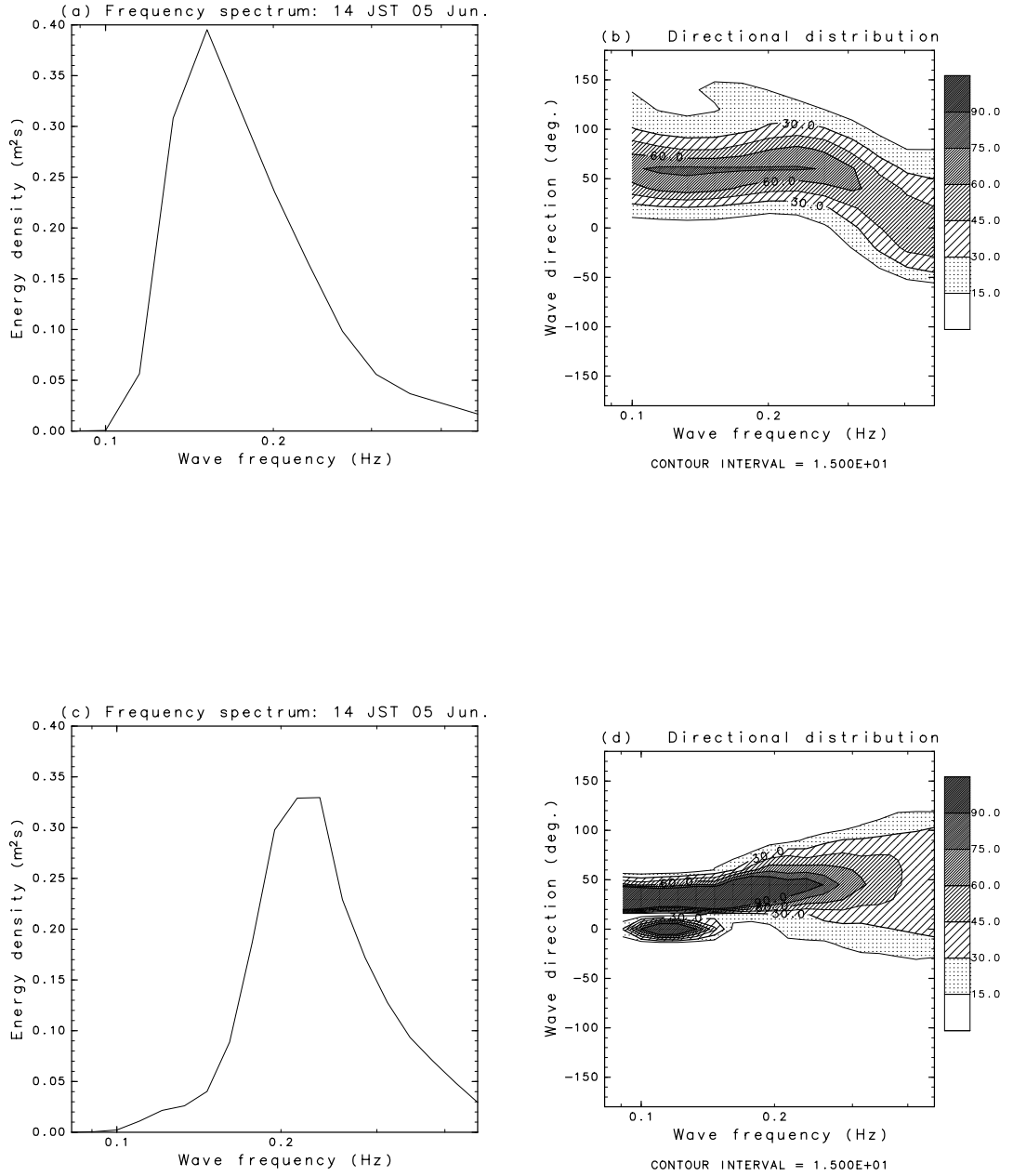

Figure 2. (a) HF radar-estimated frequency spectrum $P(f)$, and (b) directional distribution $F(f,\theta)/P(f)$ (%) at 14 JST 5 June, 2001. (c) Same as (a) but for model-predicted frequency spectrum. (d) Same as (b) but for model-predicted directional distribution.

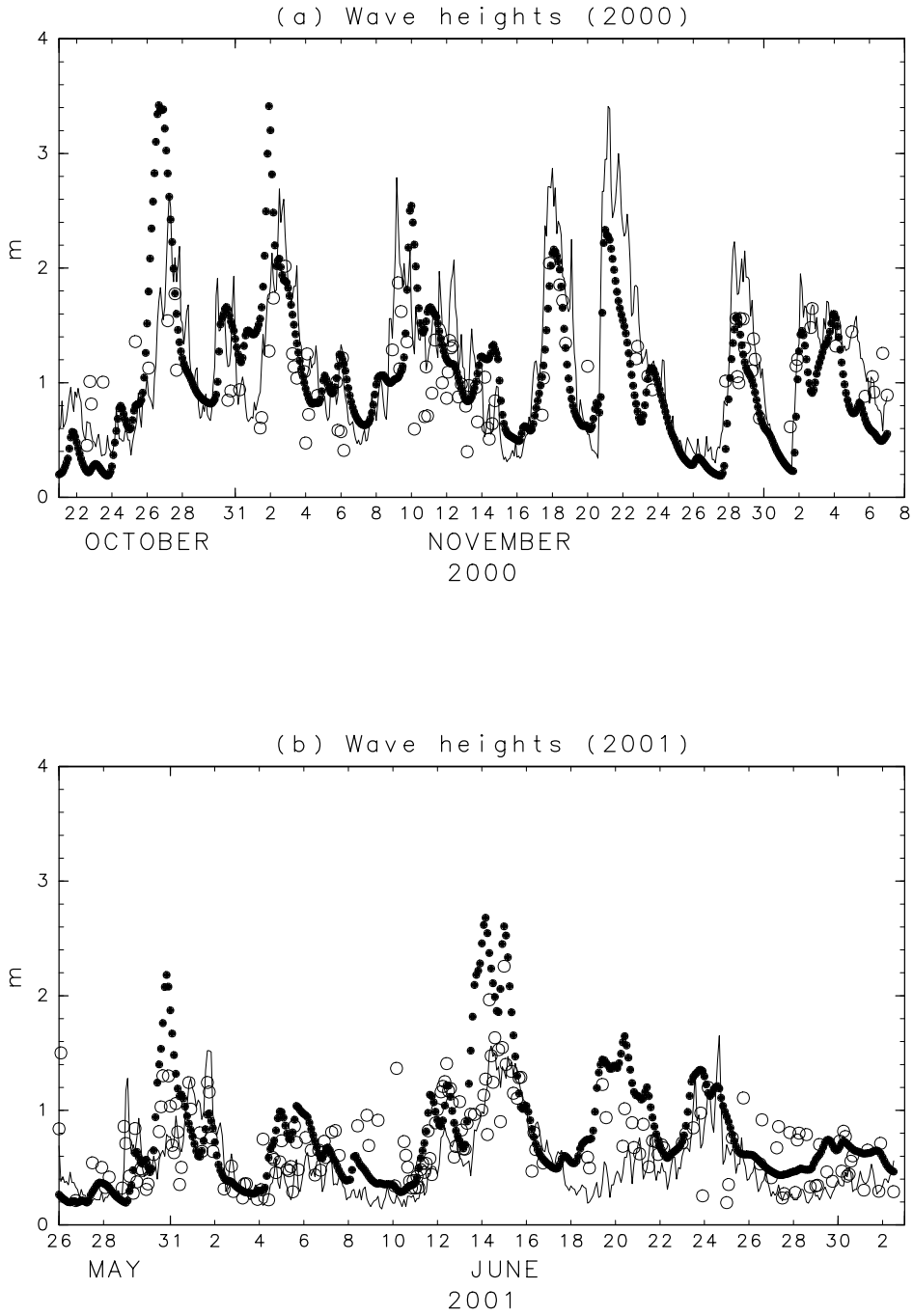

Figure 3. Time series of in-situ observed (solid line), model-predicted (black circles), and radar-estimated (white circles) wave heights in (a) 2000 and (b) 2001.

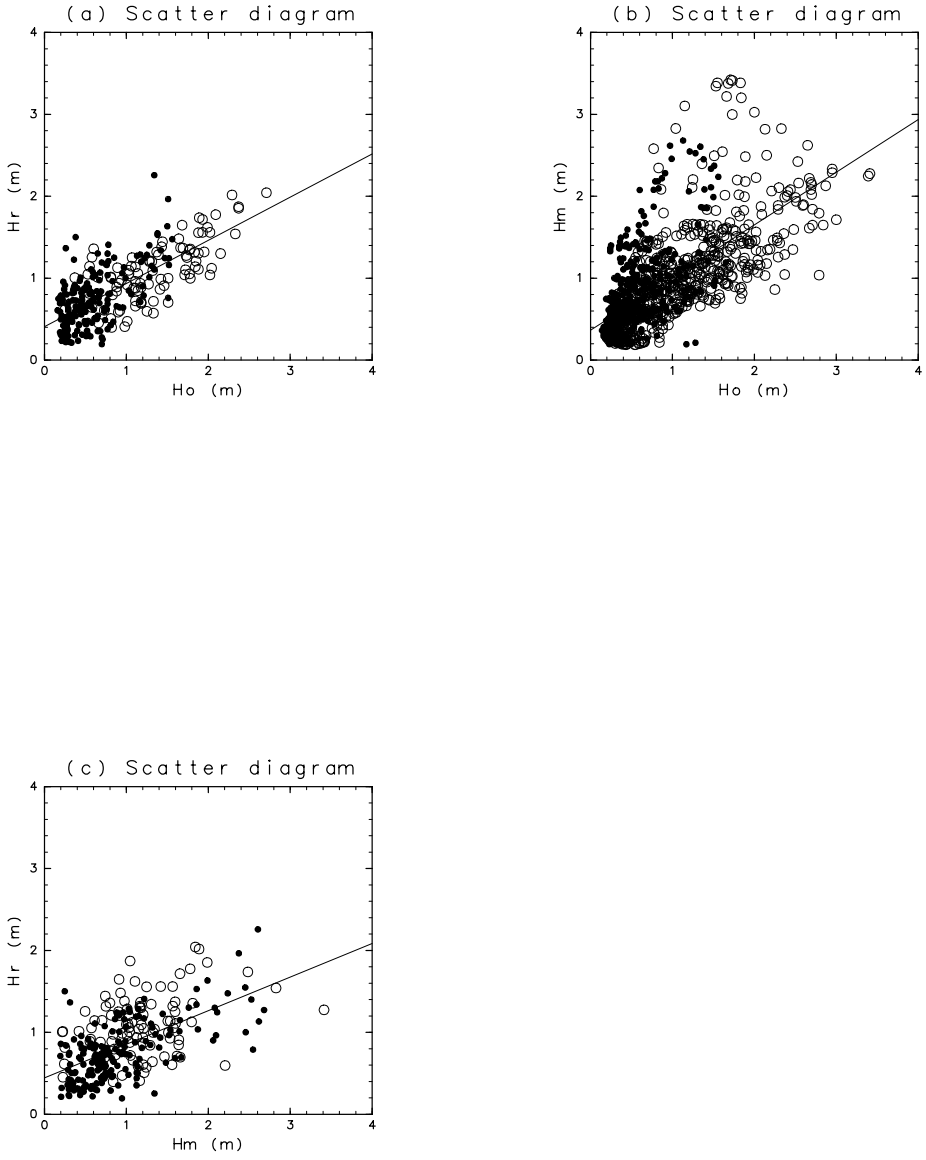

Figure 4. Scatter diagram between in-situ observed wave heights (H_o) and radar-estimated wave heights (H_r), between in-situ observed wave heights (H_o) and model-predicted wave heights (H_m), and between H_m and H_r. White circles: 2000, Black circles: 2001.

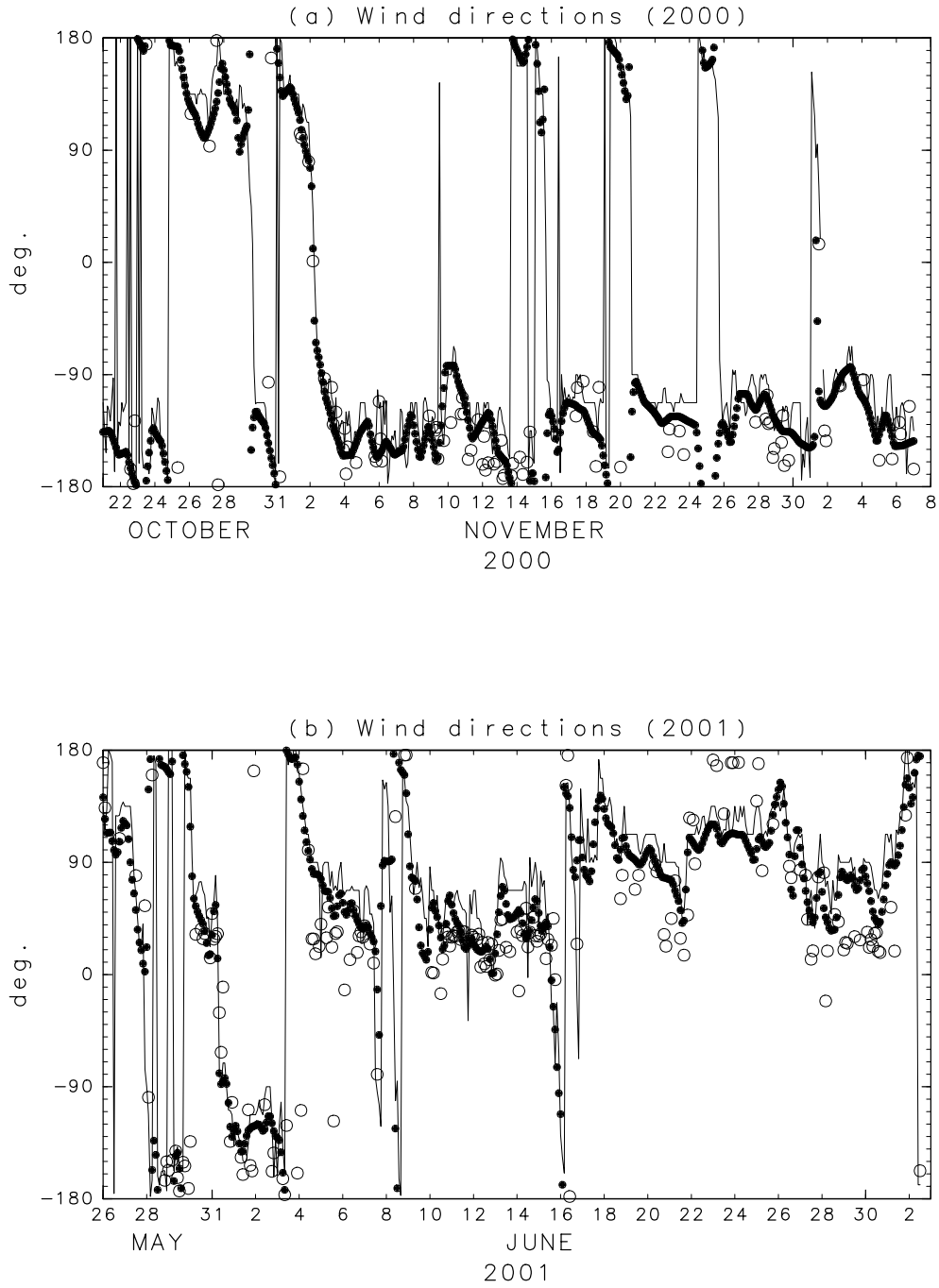

Figure 5. Same as Figure 3 but for wind directions.

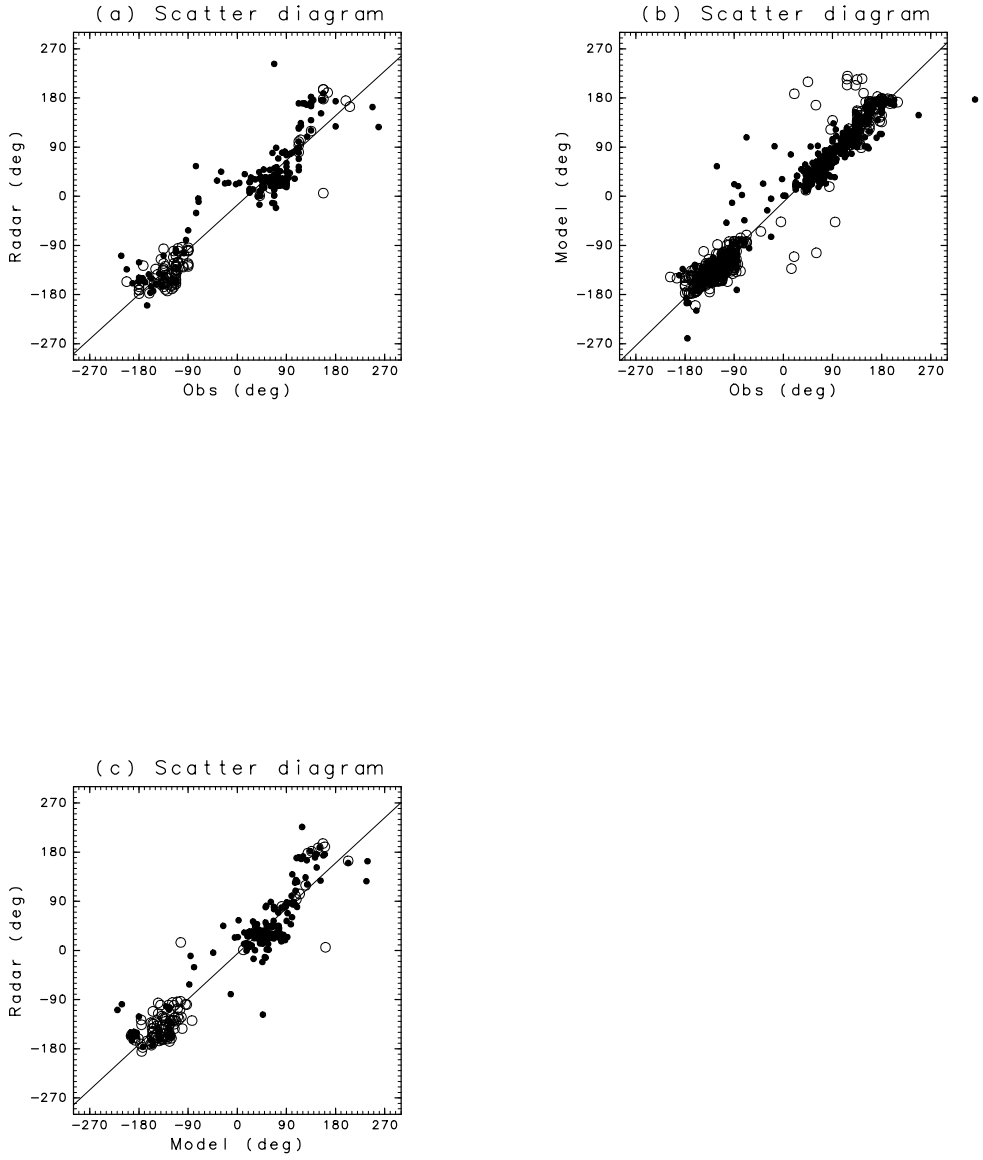

Figure 6. Same as Figure 4 but for wind directions.

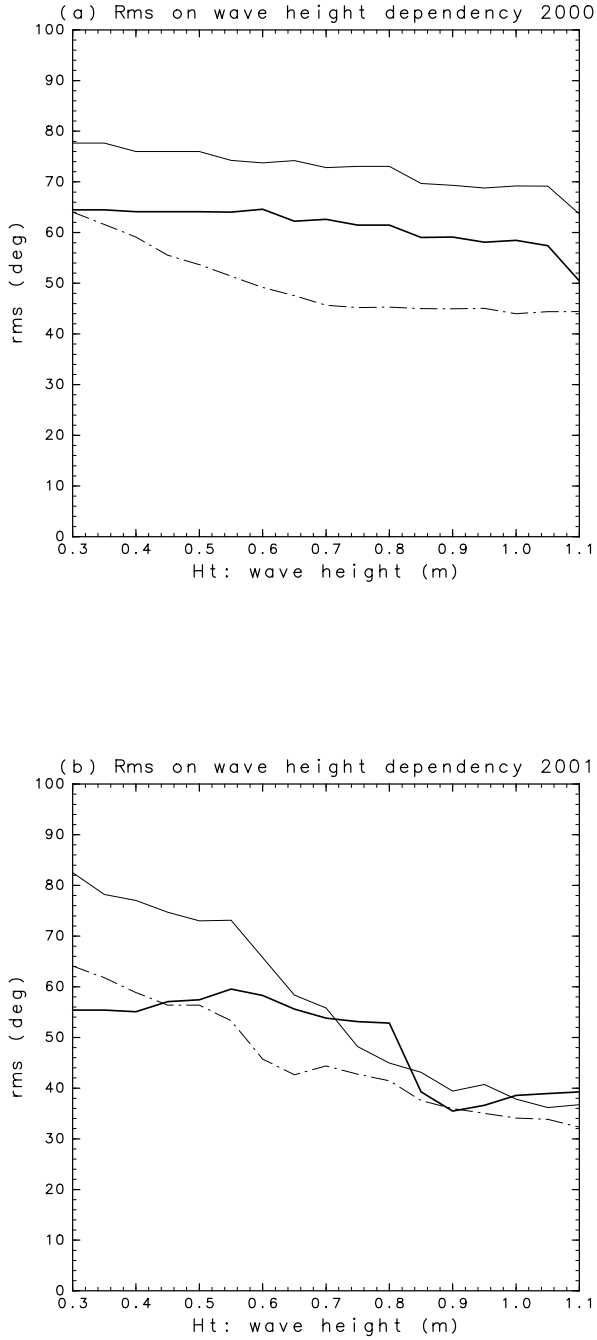

Figure 7. Rms differences of mean directions as a function of H_t, which satisfies $H_o \geq H_t$, where H_o is in-situ observed wave heights. Thick solid line: rms difference between radar-estimated and in-situ observed mean wave directions. Thin solid line: rms difference between radar-estimated and model-predicted mean wave directions. Dash-dotted line: rms difference between in-situ observed and model-predicted mean wave directions.

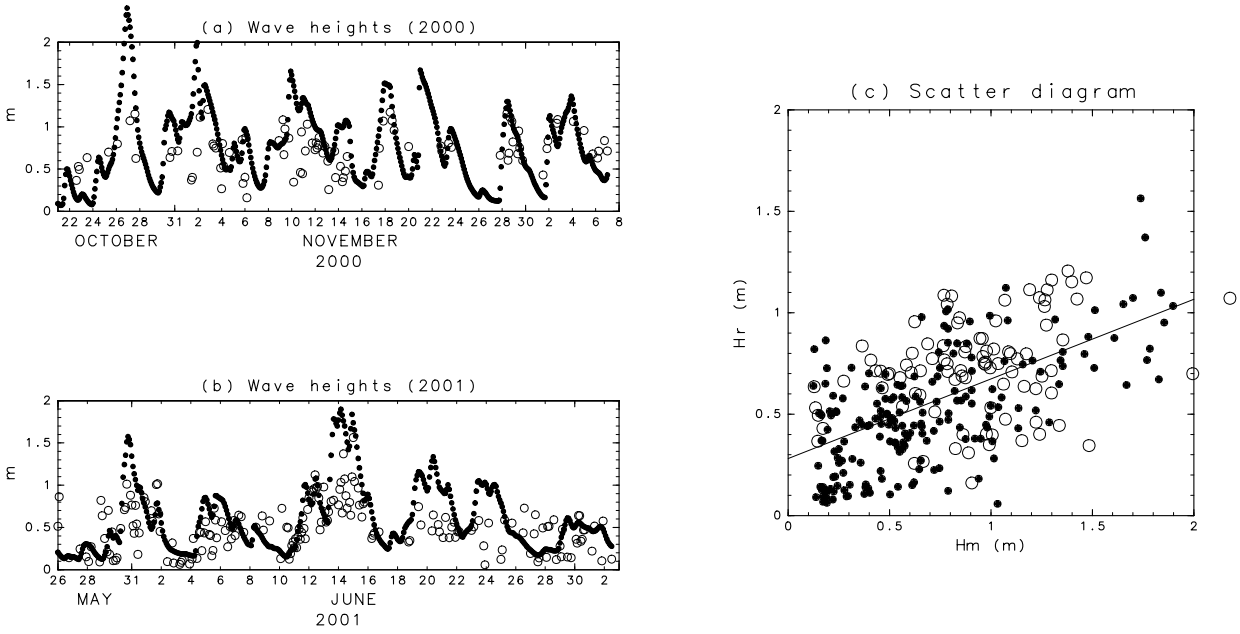

Figure 8. Time series of model-predicted (black circles), and radar-estimated (white circles) intermediate frequency wave heights ($H(f_1, f_2)$ in Eq. (10) and $(f_1, f_2) = (0.14, 0.3)$ Hz) in (a) 2000 and (b) 2001. (c) Scatter diagram of model-predicted (horizontal axis) and radar-estimated intermediate frequency wave heights. White circles: 2000, Black circles: 2001.

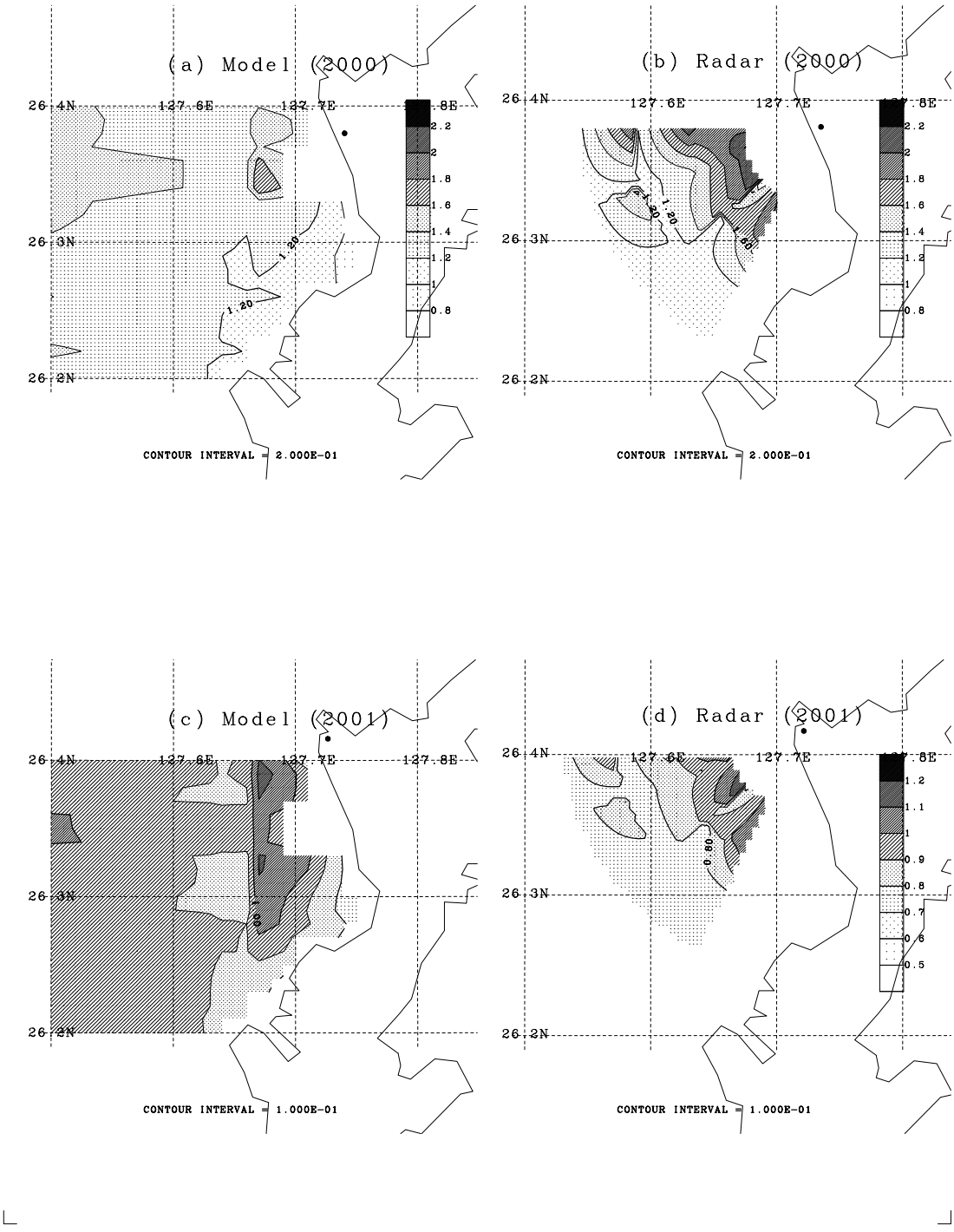

Figure 9. Mean wave heights during the HF radar observation period. (a) Model predicted wave heights ($\bar{H}_m$) in 2000, (b) radar-estimated wave heights ($\bar{H}_r$) in 2000, (c) same as (a) but in 2001, and (d) same as (b) but in 2001.

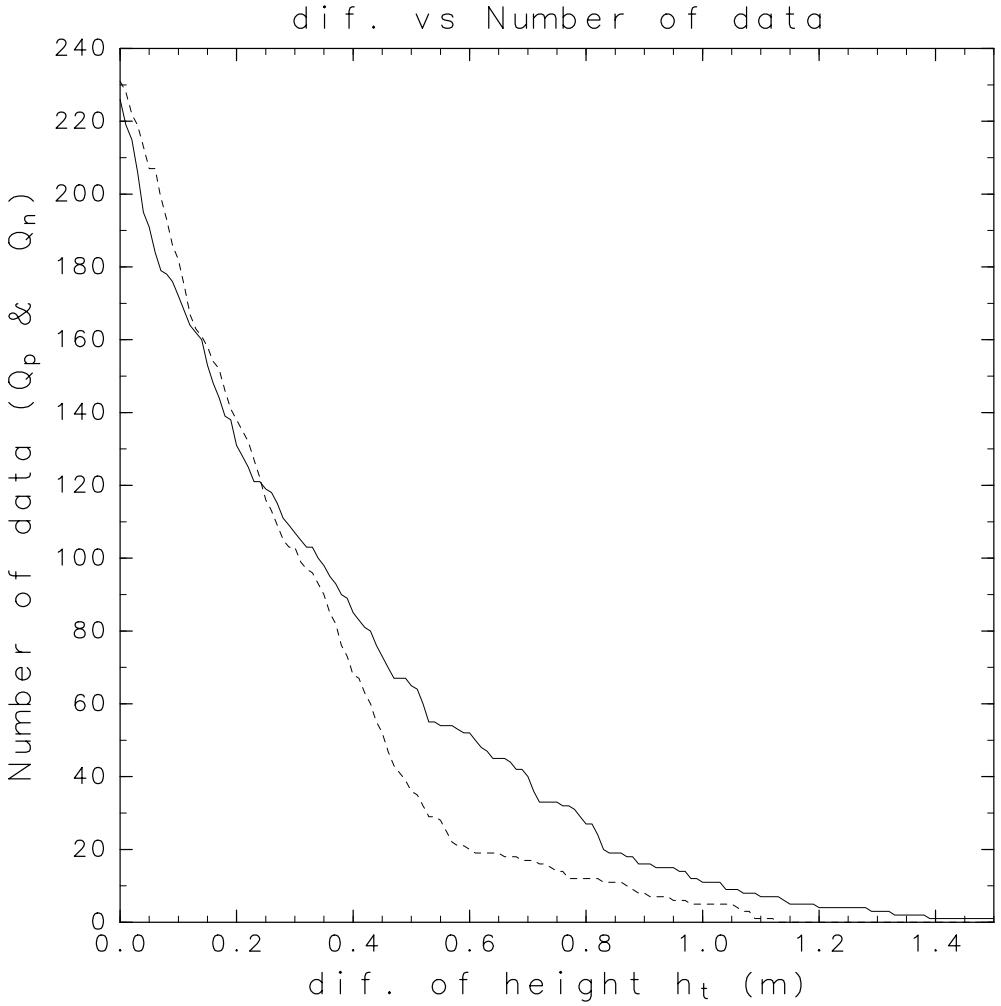

Figure 10. Numbers of positive and negative q_s defined in Eq. (15) as a function of h_t, which satisfies $H_o - H_m > h_t$. Solid line: Q_p, Dotted line: Q_n.

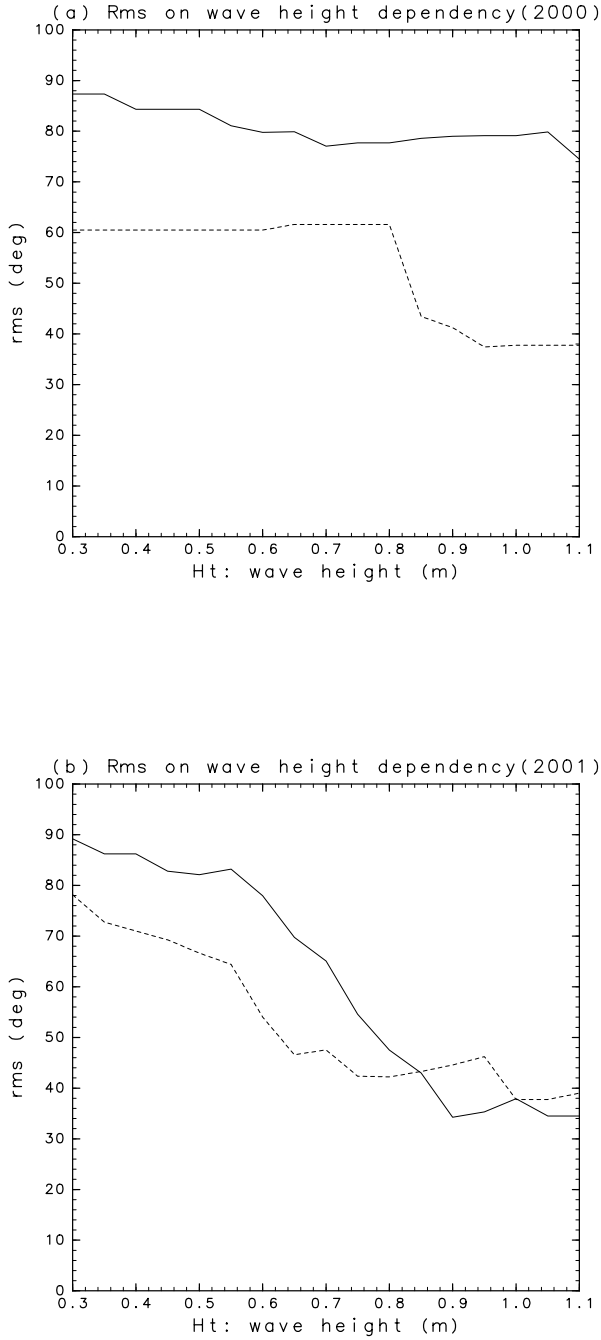

Figure 11. Rms differences of mean directions as a function of H_t, which satisfies $H_o \geq H_t$, where H_o is in-situ observed wave heights. Solid line: $q_s > 0$ (Eq. (15)), dashed line: $q_s < 0$.

Tables and captions

Table 1. Correlations (r) of in-situ observed wave parameters, HF ocean radar-derived wave parameters and model-predicted wave parameters. The values were estimated at the time when the waves were estimated from the radar. The values in the parenthesis are those estimated from the total HF radar observation period. H_o: in-situ observed wave height, H_m: model-predicted wave height, H_r: radar-derived wave height, T_{ms}: in-situ observed mean wave period, T_{mm}: model-predicted spectral mean wave period, T_{mr}: radar-derived spectral mean wave period.

	Correlation (2000)	Correlation (2001)	Correlation (Total)
$H_o - H_m$	0.55 (0.69)	0.67 (0.62)	0.61 (0.67)
$H_o - H_r$	0.70	0.64	0.73
$H_m - H_r$	0.32	0.64	0.58
$T_{ms} - T_{mm}$	0.56 (0.45)	0.58 (0.48)	0.59 (0.47)
$T_{ms} - T_{mr}$	0.47	0.37	0.50
$T_{mm} - T_{mr}$	0.13	0.31	0.31

Table 2. Rms differences of in-situ observed wave parameters, HF ocean radar-derived wave parameters and model-predicted wave parameters. The values were estimated at the time when the waves were estimated from the radar. The values in the parenthesis are those estimated from the total HF radar observation period. θ_{ws}: in-situ observed wind direction, θ_{wm}: model input wind direction, θ_{wr}: radar-derived wind direction. θ_{ms}: in-situ observed mean wave direction, θ_{mm}: model-predicted spectral mean wave period, θ_{mr}: radar-derived spectral mean wave direction.

	rms dif.(2000)	rms dif.(2001)	rms dif. (Total)
$H_o - H_m$	0.52 m(0.50 m)	0.51 m (0.46 m)	0.51 m (0.48 m)
$H_o - H_r$	0.45 m	0.33 m	0.38 m
$H_m - H_r$	0.55 m	0.45 m	0.48 m
$\theta_{ws} - \theta_{wm}$	25.1° (26.9°)	24.3° (28.9°)	24.5° (27.8°)
$\theta_{ws} - \theta_{wr}$	30.7°	44.1°	40.2°
$\theta_{wm} - \theta_{wr}$	30.8°	37.5°	35.4°
$\theta_{ms} - \theta_{mm}$	53.6° (65.0°)	72.5°(70.6°)	66.8°(67.5°)
$\theta_{ms} - \theta_{mr}$	77.4°	86.3°	83.5°
$\theta_{mm} - \theta_{mr}$	64.8°	56.6°	53.5°
$T_{mm} - T_{mr}$	1.56 s	1.32 s	1.40 s

Table 3. Correlations between HF ocean radar-derived and model-predicted $H(f_1, f_2)$ (Eq. (10)) for low ($(f_1, f_2) = (0, 0.14)$ Hz), intermediate ($(f_1, f_2) = (0.14, 0.3)$ Hz), and high $(f_1, f_2) = (0.3, 0.5)$ Hz) frequency bands

	2000	2001	Total
low	0.27	0.55	0.48
intermediate	0.32	0.64	0.59
high	0.29	0.41	0.39

Table 4. Rms differences between HF ocean radar-derived and model-predicted $\theta_m(f_1, f_2)$ (Eq. (11)) for low, intermediate, and high frequency bands

	2000	2001	Total
low	85.3°	65.4°	73.5°
intermediate	67.4°	57.7°	61.1°
high	43.9°	51.4°	49.0°